Materials Research Bulletin 83 (2016) 217–224

Contents lists available at ScienceDirect

Materials Research Bulletin

journal homepage: www.elsevier.com/locate/matresbu

WO_3/TiO_2 composite coatings: Structural, optical and photocatalytic properties

Zorana Dohčević-Mitrović[a,*], Stevan Stojadinović[c], Luca Lozzi[d], Sonja Aškrabić[a], Milena Rosić[e], Nataša Tomić[a], Novica Paunović[a], Saša Lazović[b], Marko G. Nikolić[b], Sandro Santucci[d]

[a] Center for Solid State Physics and New Materials, Institute of Physics Belgrade, University of Belgrade, Pregrevica 118, 11080 Belgrade, Serbia
[b] Institute of Physics Belgrade, University of Belgrade, Pregrevica 118, 11080 Belgrade, Serbia
[c] Faculty of Physics, University of Belgrade, Studentski Trg 12-16, 11000 Belgrade, Serbia
[d] Department of Physical and Chemical Sciences, University of L'Aquila, Via Vetoio 67100, L'Aquila, Italy
[e] Laboratory for Material Science, Institute of Nuclear Sciences, Vinča, University of Belgrade, P.O. Box 522, 11001 Belgrade, Serbia

ARTICLE INFO

Article history:
Received 24 February 2016
Received in revised form 19 May 2016
Accepted 6 June 2016
Available online 7 June 2016

Keywords:
A. Nanostructures
A. Oxides
D. Crystal structure
B. Optical properties
D. Catalytic properties

ABSTRACT

WO_3/TiO_2 and TiO_2 coatings were prepared on titania substrates using facile and cost-effective plasma electrolytic oxidation process. The coatings were characterized by X-ray diffraction, scanning electron microscopy, Raman, UV–vis diffuse reflectance spectroscopy, and X-ray photoelectron spectroscopy. With increasing duration of PEO process, the monoclinic WO_3 phase became dominant and new monoclinic $WO_{2.96}$ phase appeared. The optical absorption edge in the WO_3/TiO_2 samples, enriched with $WO_3/WO_{2.96}$ phase, was shifted to the visible region. The photocatalytic efficiency of WO_3/TiO_2 and pure TiO_2 samples was evaluated by performing the photodegradation experiments in an aqueous solution of Rhodamine 6G and Mordant Blue 9 under the visible and UV light. The WO_3/TiO_2 catalysts are much more efficient than pure TiO_2 under visible light and slightly better under UV light. The improvement of photocatalytic activity in the visible region is attributed to better light absorption, higher adsorption affinity and increased charge separation efficiency.

1. Introduction

Among semiconductor materials, titanium dioxide (TiO_2) in anatase phase has been shown as excellent and widely used photocatalyst for the degradation of different organic contaminants, because of its physical and chemical stability, high oxidative power, high catalytic activity, long-term photostability, low cost and ease of production. Many organic compounds can be decomposed in an aqueous solution in the presence of TiO_2, illuminated by photons with energies greater than or equal to the band gap energy of titanium dioxide (3.2 eV for anatase TiO_2) [1–6]. The major drawback for TiO_2 commercial use lies in its wide band gap, and relatively high recombination rate of photoinduced electron-hole pairs. The modification of TiO_2 by doping with metals and non-metals [7–12] or by Ti^{3+} self-doping [13,14] have been extensively performed in order to improve its photocatalytic activity under the visible irradiation.

Another very promising approach is the combination of TiO_2 with metal oxides like V_2O_5, ZnS, $InVO_4$, WO_3 [15–19] or graphene [20]. Among the metal oxides, WO_3 has smaller band gap (2.8 eV) than TiO_2 and better absorbs visible light. Moreover, WO_3 has a suitable conduction band potential and acts as a trapping site for photoexcited electrons from TiO_2. The photogenerated holes from the valence band of WO_3 move towards and accumulate in the valence band of TiO_2. In such a way the efficiency of charge separation is increased, enhancing at the same time the photocatalytic acivity of TiO_2 [21]. Additionally, the formation of WO_3 monolayer on TiO_2 increases the acidity of the WO_3/TiO_2 surface enabling the adsorption of greater amount of hydroxyl groups and organic reactants on the surface [21,22]. In recent years, WO_3/TiO_2 composites were synthesized using different methods such as sol-gel, ultrasonic spray pyrolysis, ball milling, hydrothermal, sol-precipitation, and impregnation to improve photocatalytic activity of TiO_2 under the visible light [23–28]. Thin films of TiO_2/WO_3 have also been prepared by dip and spin coating [29,30] or by one-step oxidation method [31]. In most of these reports it was demonstrated that WO_3/TiO_2 composites were found to have much

* Corresponding author
E-mail address: zordoh@ipb.ac.rs (Z. Dohčević-Mitrović).

http://dx.doi.org/10.1016/j.materresbull.2016.06.011
0025-5408/

higher photocatalytic activity under the visible light than pure TiO_2 [24,26,28,31]. Therefore, the combination of these two materials can lead to increased charge carrier lifetime and improved photocatalytic activity under the visible irradiation. Among different synthesis routs, plasma electrolytic oxidation (PEO) process is very facile, cost-effective and environmentally benign process for producing of well-adhered and crystalline oxide films, but the studies on structural and photocatlytic properties of WO_3/TiO_2 films (coatings), produced by PEO process, are limited [32–34].

In this study WO_3/TiO_2 coatings were synthetized on titanium substrate by using PEO process. Structural and optical properties of the coatings were fully characterized by XRD, SEM, Raman, XPS, and diffuse reflectance spectroscopy. The aim of this work was to tailor the band gap energy of WO_3/TiO_2 coatings towards the visible spectral region, varying the time of PEO process and to explore the photocatalytic properties of the coatings. The photocatalytic efficiency of WO_3/TiO_2 coatings was tested under the visible and UV light irradiation using Rhodamine 6G and Mordant Blue 9 as model pollutants. We demonstrated that this approach provides an efficient route for the formation of cost-effective and improved visible-light-driven photocatalysts.

2. Experimental

2.1. Preparation of WO_3/TiO_2 coatings

WO_3/TiO_2 coatings were prepared on titanium substrate using plasma electrolytic oxidation (PEO) process. PEO process is an anodizing process of lightweight metals (aluminum, magnesium, zirconium, titanium, etc.) or metal alloys above the dielectric breakdown voltage, when thick, highly crystalline oxide coating with high corrosion and wear resistance, and other desirable properties are produced. During the PEO process, numerous small sized and short-lived discharges are generated continuously over the coating's surface, accompanied by gas evolution. Due to increased local temperature, plasma-chemical reactions are induced at the discharge sites modifying the structure, composition, and morphology of such oxide coatings. The oxide coatings formed by PEO process usually contain crystalline and amorphous phases with constituent species originating both from metal and electrolyte. WO_3/TiO_2 coatings were formed on the rectangular titanium samples (99.5% purity, Alfa Aesar) of dimensions 25 mm $\times$ 10 mm $\times$ 0.25 mm, which were used as working electrodes in the experiment. The working electrodes were sealed with insulation resin leaving only an area of 1.5 cm^2 as an active surface. Before starting the PEO process, titanium samples were degreased in acetone, ethanol, and distilled water, using ultrasonic cleaner and dried in a warm air stream. The anodic oxidation process was conducted in an aqueous solution of 10^{-3} M 12-tungstosilicic acid ($H_4SiW_{12}O_{40}$), at constant current density (150 mA/cm^2). During PEO process, the electrolyte circulated through the chamber–reservoir system. The temperature of the electrolyte was kept fixed at (20 $\pm$ 1) °C. Detailed description of PEO process is given in the ref. [33].

After plasma electrolytic oxidation, the samples were rinsed in distilled water to prevent additional deposition of electrolyte components during drying. The WO_3/TiO_2 samples were obtained by varying the time of PEO process from 90 s up to 300 s. The pure TiO_2 sample was obtained after 300 s of PEO process.

2.2. Characterization of WO_3/TiO_2 coatings

The crystal structure of WO_3/TiO_2 samples was analyzed by X-ray diffraction (XRD), using a Rigaku Ultima IV diffractometer in Bragg-Brentano geometry, with Ni-filtered CuKα radiation (λ = 1.54178 Å). Diffraction data were acquired over the scattering angle 2θ from 15° to 75° with a step of 0.02° and acquisition rate of 2°/min. The XRD spectra refinement was performed with the software package Powder Cell. The TCH pseudo-Voigt profile function gave the best fit to the experimental data.

Scanning electron microscope (SEM) JEOL 840A equipped with an EDS detector was used to characterize the morphology and chemical composition of formed oxide coatings.

Micro-Raman scattering measurements were performed at room temperature in a backscattering geometry, using a Jobin-Yvon T64000 triple spectrometer system and Nd:YAG laser line of 532 nm as an excitation source. The incident laser power was kept less than 10 mW in order to prevent the heating effects.

UV-vis diffuse reflectance spectra were acquired using the Specord M40 Carl Zeiss spectrometer.

X-ray photoelectron spectroscopy (XPS) was used for the surface composition analysis of WO_3/TiO_2 coatings. XPS was carried out on a VG ESCALAB II electron spectrometer with a base pressure in the analysis chamber of 10^{-8} Pa. The X-ray source was monochromatized AlKα radiation (1486.6 eV) and the instrumental resolution was 1 eV. The spectra were calibrated using the C 1 s line (284.8 eV) of the adventitious carbon and corrected by subtracting a Shirley-type background.

2.3. Photocatalytic experiments

The photocatalytic activity of WO_3/TiO_2 samples was evaluated by monitoring the decomposition of Rhodamine 6G (R6G) and Mordant Blue 9 (MB9) under the irradiation of two different light sources: fluorescent and UV lamps. The photocatalytic measurements on R6G solution (initial concentration in water: 10 mg/L) have been performed using a 36 W visible fluorescent lamp (Hyundai eagle), whose emission spectrum, compared to sunlight spectrum, is given in Ref. [9]. The cuvette (3 mL) was placed at about 5 cm from the lamp. The evolution of the rhodamine concentration was followed by measuring the variation of the intensity of main absorption peak at ~525 nm. UV–vis absorption measurements as a function of the light exposure time were performed by using USB2000 spectrometer by Ocean Optics. The solution was placed in the dark for 60 min to reach the adsorption/desorption equilibrium before visible light exposure.

The photocatalytic activity of WO_3/TiO_2 samples under UV light irradiation was evaluated using aqueous solution of MB9 as a model pollutant. Batch type experiments were performed in an open thermostated cell (at 25 °C). The cell was equipped with a water circulating jacket to maintain the solution at room temperature. A mercury lamp (125 W) was used as a light source and was placed 13 cm above the surface of the dye solution. The initial concentration of MB9 in an aqueous suspension was 50 mg/L and the working volume was 25 mL. Before the lamp was switched on, the cell was kept in dark for 60 min in order to achieve the adsorption-desorption equilibrium. At regular time intervals the aliquots were taken and the concentration of the dye was determined by UV–vis spectrophotometer (Super Scan) at λ_{max} = 516 nm. The photocatalytic experiments were conducted at the natural pH of the dyes (pH = 7 in a case of R6 G solution and at pH = 6 in a case of MB9 solution). All photocatalytic measurements were repeated at least twice to check their reproducibility.

In order to detect the formation of free hydroxyl radicals ($OH^•$) on the UV illuminated WO_3/TiO_2 surface, photoluminescence (PL) measurements were performed using terephthalic acid, which is known to react with $OH^•$ radicals and produces highly fluorescent 2-hydroxyterephthalic acid. The experiment was conducted at ambient temperature. The WO_3/TiO_2 photocatalyst (TW300) was placed in open termostated cell filled with 20 mL of the 5×10^{-4} mol L^{-1} terephthalic acid in a diluted NaOH aqueous solution with

a concentration of 2×10^{-3} mol L^{-1}. UV lamp (125 W) was used as a light source. Sampling was performed after 15, 30, 60 and 90 min. PL spectra of reaction solution, using excitation wavelength of 315 nm, were measured on a Spex Fluorolog spectrofluorometer system at wavelength of 425 nm for which the 2-hydroxytereph-thalic acid exhibits intense PL peak.

3. Results and discussion

3.1. Crystal structure and morphology

XRD patterns of the WO_3/TiO_2 samples obtained for 90 (TW90), 120 (TW120), and 300 s (TW300) of PEO process are presented in Fig. 1. The diffraction peaks which appear in TW90 sample at $2\theta = 23.3°$, 33.4°, 54.2° belong to (002), (022) and (042) planes of monoclinic WO_3 phase, which crystallizes in $P2_1/c$ (No. 14) space group. Besides these XRD peaks, the XRD pattern also shows peak at 25.3° which belongs to TiO_2 anatase crystal phase (space group $I4_1/amd$ (No. 141)) and intense peaks of elemental Ti (space group $P6_3/mmc$ (No. 194)). This indicates that Ti substrate is not completely oxidized to form TiO_2 during the PEO process. With increasing duration of PEO process, for the TW120 and TW300 samples, the XRD peaks of WO_3 phase became more intense. The spectra refinement, using Powder Cell program, showed that besides WO_3 phase a monoclinic $WO_{2.96}$ phase appeared (space group $P2/c$ (No. 13)). Furthermore, the intensities of XRD peaks which belong to TiO_2 phase and elemental Ti decreased implying that the WO_3/TiO_2 coatings were enriched with $WO_3/WO_{2.96}$ phase. According to the JCPDS database for WO_3, $WO_{2.96}$, TiO_2, and elemental Ti (JCPDS: 43-1035 (WO_3), 30-1387 ($WO_{2.96}$), 16-0934 (TiO_2) and 44-1294 (elemental Ti)) very good agreement is obtained between experimental and calculated diffraction patterns of the WO_3/TiO_2 samples. In Fig. 1 are marked main XRD peaks of WO_3 and $WO_{2.96}$ phases for clarity. The lattice parameters and the estimated volume fractions (%) of different phases for the WO_3/TiO_2 samples are given in Table 1.

In Fig. 2 are presented SEM images of WO_3/TiO_2 samples. In the TW90 sample produced with shorter PEO time, certain number of microdischarge channels together with molten regions was present because of the rapid cooling of the electrolyte. With increasing time of PEO process, when the thickness of the oxide coating was increased, the number of microdischarge channels and micropores decreased followed by increased roughness of the coating's surface.

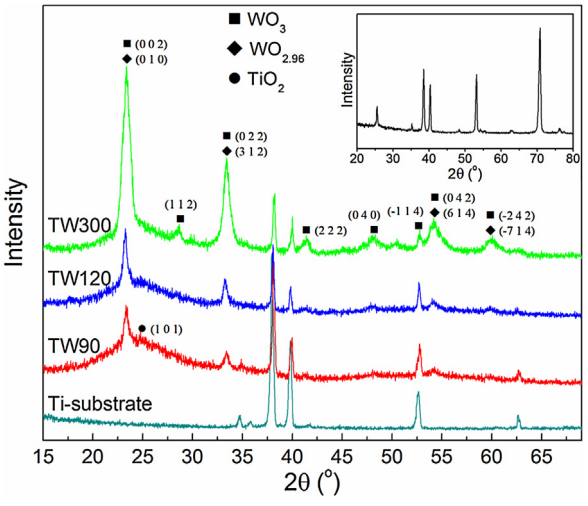

Fig. 1. XRD patterns of TW90, TW120 and TW300 samples formed in various stages of PEO process, together with the XRD spectrum of Ti-substrate. In the inset is given XRD spectrum of anatase TiO_2 obtained on Ti-substrate after 300 s of PEO process.

Table 1
Phase fraction (vol%) and cell parameters (Å) of WO_3/TiO_2 samples.

Phase	TW90	TW120	TW300
WO_3	$a = 7.4060$ $b = 7.6400$ $c = 7.6455$ 29.6%	$a = 7.3026$ $b = 7.5398$ $c = 7.6933$ 29.1%	$a = 7.4060$ $b = 7.5177$ $c = 7.5920$ 54.5%
$WO_{2.96}$	/	$a = 11.9006$ $b = 3.8258$ $c = 59.6312$ 36.70%	$a = 11.8000$ $b = 3.8098$ $c = 59.7400$ 20.90%
TiO_2	$a = 3.7778$, $c = 9.4440$, 66.0%	$a = 3.7841$, $c = 9.5105$, 32.2%	$a = 3.7790$ $c = 9.4124$ 23.8%
Ti	$a = 2.9481$ $c = 4.7325$ 4.3%	$a = 2.9594$ $c = 4.7254$ 2.0%	$a = 3.0510$ $c = 4.7820$ 0.9%

The quantitative elemental analysis confirmed the presence of Ti, O and W and the elemental composition of the samples is shown in Table 2. EDS analysis confirmed the increasing trend of W content with increasing of PEO time.

3.2. Raman and diffuse reflectance spectra

The Raman spectra of WO_3/TiO_2 samples produced for different duration of PEO process are shown in Fig. 3a. Several modes originating from two crystalline oxide phases can be identified (marked on Fig. 3a as T and W).

The Raman modes positions were determined using Lorentzian fit procedure and the deconvoluted spectra of TW90, TW120 and TW300 samples are presented in Fig. 3b. Besides the modes at about 144 cm^{-1} ($E_{g(1)}$), 197 cm^{-1} ($E_{g(2)}$), 393 cm^{-1} ($B_{1g(1)}$), 516 cm^{-1} (A_{1g}, $B_{1g(2)}$) and 638 cm^{-1} ($E_{g(3)}$) which belong to anatase phase of TiO_2 [35], several modes characteristic for monoclinic WO_3 phase are present [22,36,37]. The broad band at ~703 cm^{-1} and strong band at ~793 cm^{-1} are assigned to the stretching (O–W–O) modes of the bridging oxygen of the WO_6 octahedra. The bands observed at ~272 cm^{-1} and at ~316 cm^{-1} are assigned to the bending (O—W—O) vibrations of bridging oxygen in monoclinic m-WO_3 [22,37]. The band positioned at ~989 cm^{-1} is assigned to the dioxo $(W{=}O)_2$ symmetric vibration of the isolated surface WO_4 structure, whereas its weak shoulder at ~942 cm^{-1} represents asymmetric vibration of the same atomic group [22,37]. The low frequency mode at 58 cm^{-1} belongs to the to lattice modes of monoclinic WO_3 phase [38].

Further, from the Lorentzian fit procedure it was obtained that the ratio between the intensity of the peak positioned at 639 cm^{-1} and the sum of the intensities of the 703 cm^{-1} and 793 cm^{-1} peaks decreased with the increase of PEO time. This fact supports the XRD results that WO_3 content increases with prolonged duration of PEO process.

In Fig. 4 are presented the Raman spectra of TW90, TW120 and TW300 samples in the C—H and O—H region. The Raman band at around 2885 cm^{-1} originates from the overlapped CH_3 and CH_2 stretching vibrations [39]. Broad Raman peak in the 3000–3600 cm^{-1} frequency range can be assigned to the O—H stretching vibration of water molecules adsorbed on the surface of the WO_3/TiO_2 coatings [3,5].

The absorption spectra of TW90, TW120 and TW300 samples are given in Fig. 5a. With increasing content of WO_3 phase the absorption edge shifts to higher wavelengths. In the spectra of TW120 a structure around 380–400 nm can be observed, which is

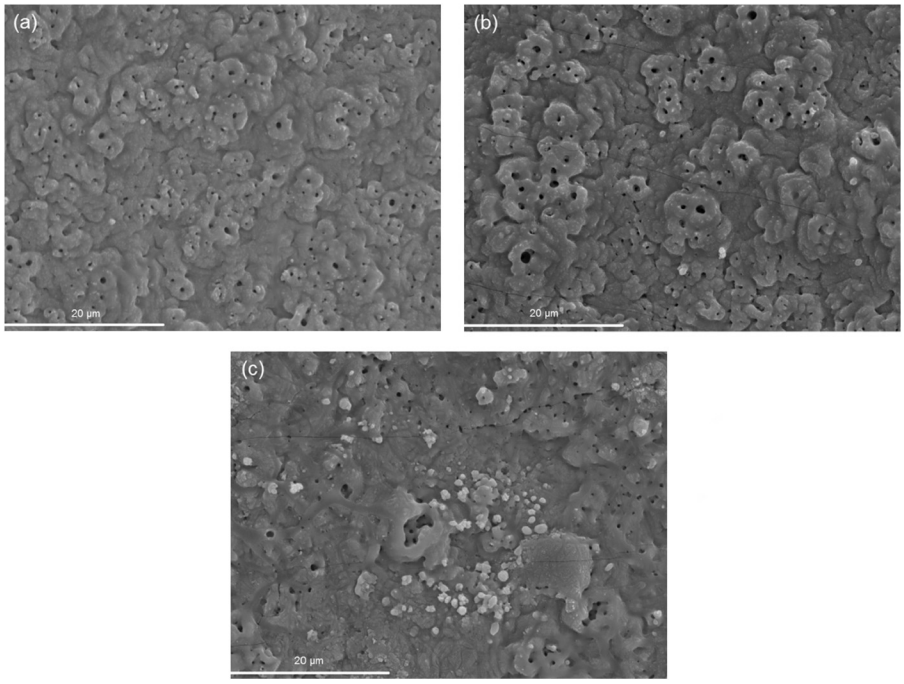

Fig. 2. SEM micrographs of WO_3/TiO_2 samples formed in various stages of PEO process: (a) TW90, (b) TW120 and (c) TW300 sample.

very pronounced in the TW300 sample. The appearance of this absorption structure can be attributed to the electronic population of WO_3 conduction band [40]. From the absorption spectra from Fig. 4a, applying the same procedure as Ghobadi in his work [41], the band gap energies for pure TiO_2 and WO_3/TiO_2 samples were estimated. In Fig. 5b are presented the Tauc plots for indirect transition, as TiO_2 and WO_3 are indirect band gap semiconductors [26]. The band gap (E_g) energies are 3.19 eV for pure TiO_2, and 2.84, 2.77 and 2.6 eV for TW90, TW120 and TW300 samples, respectively. It is obvious that with increasing WO_3 content the band gap decreases compared to pure TiO_2 and shifts to the visible spectral range. Patrocinio et al. [40] have shown that in TiO_2/WO_3 films, the WO_3 conduction band introduces new low lying electronic levels with respect to the conduction band of TiO_2, causing the lowering of the band gap energy of composite samples compared to pure TiO_2. This finding is in accordance with the band gap behavior of our WO_3/TiO_2 samples from Fig. 5b.

3.3. XPS analysis

The XPS study was further used to confirm the chemical binding states of W 4f. The W 4f XPS spectra of the TW90 and TW300 samples and the results of their decomposition into peaks are shown in Fig. 6. The W 4f spectrum of TW90 sample (Fig. 6a) can be deconvoluted into one doublet with binding energies of 35.8 (W $4f_{7/2}$) and 38.1 eV (W $4f_{5/2}$), respectively. The energy position of this doublet corresponds to the W^{6+} oxidation state [42].

In the TW300 sample (Fig. 6c) the contribution of W^{5+} states from nonstoichiometric oxide phase can be seen. The W 4f spectrum can be deconvoluted with two doublets. The first two characteristic peaks at 36 (W $4f_{7/2}$) and 38.3 eV (W $4f_{5/2}$) correspond to W^{6+} state as in the case of TW90. The binding energies of these peaks are somewhat higher than that for TW90 sample. The up-shift in binding energy can be ascribed to the presence of defects and OH-groups on the surface [43], existence of

Table 2
EDS analysis of the WO_3/TiO_2 composites.

Sample	EDS data			
	Ti (at%)	W (at%)	O (at%)	W/Ti
TW90	6.98	14.17	78.85	2.03
TW120	6.22	16.12	77.66	2.59
TW300	4.09	17.16	78.75	4.1

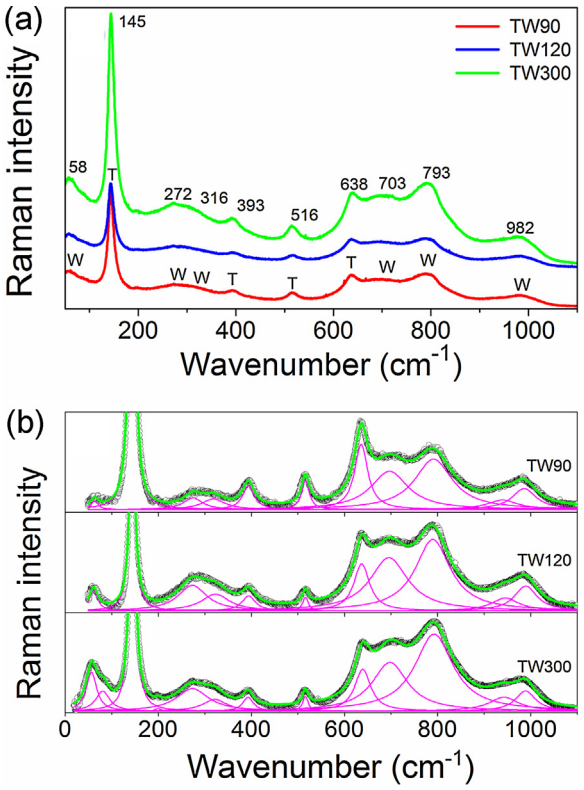

Fig. 3. Room-temperature Raman spectra of WO_3/TiO_2 samples (a). The TiO_2 and WO_3 Raman modes are marked as T and W. Deconvoluted Raman spectra of TW90, TW120 and TW300 samples (b).

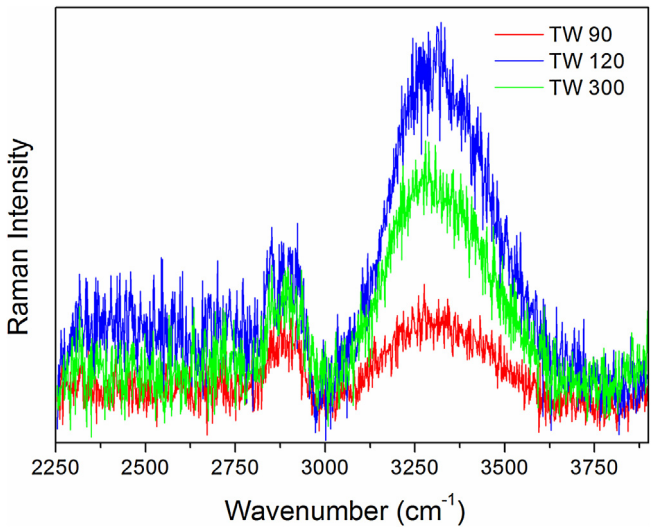

Fig. 4. Raman spectra of WO_3/TiO_2 samples in the C–H and O–H spectral region.

which is confirmed by Raman analysis (Fig. 4). The binding energies of the second doublet at 34.5 (W $4f_{7/2}$) and 36.5 eV (W $4f_{5/2}$) correspond to W^{5+} state [42]. These results are in accordance with XRD analysis.

The O 1s spectra of TW90 and TW300 samples (Fig. 6b, d) are decomposed into three peaks. The major peak at binding energy of 531.2 eV can be assigned to the oxygen atoms in WO_3 and to the OH-groups present on the surface [32,44]. The second peak observed at 530.6 eV has been attributed to oxygen bound to Ti [26], whereas the binding energy of the third peak at 533.1 eV corresponds to the oxygen in water molecules bound in the coating's structure or adsorbed on its surface [45]. The relative intensity of the XPS peaks at 531.2 eV and 533.1 eV was increased in the TW300 sample. The intensity increase of these peaks can be related to the presence of sub-stoichiometric WO_{3-x} phase ($WO_{2.96}$). Similar behavior was reported in the paper of Shpak et al. [44] in which these peaks were more intense in WO_{3-x} oxides than in stoichiometric WO_3. This finding is also supported by the Raman spectrum of TW300 sample (Fig. 4), for which the intensity of the Raman mode, corresponding to the water molecules adsorbed on the surface, is higher than in TW90 sample.

3.4. Photocatalytic performances of WO_3/TiO_2 coatings

Fig. 7a shows the kinetics of degradation of R6G for pure TiO_2 and WO_3/TiO_2 samples under the visible light. No detectable degradation of R6G was registered without the presence of WO_3/TiO_2 samples (black circles on Fig. 7a). As can be seen from Fig. 7a, both TiO_2 and WO_3/TiO_2 coatings adsorbed the dye in the equilibrium period of 60 min before the exposure to visible light. It is known from the literature that the zero point charge (pH_{zpc}) of TiO_2 lies between 6 and 6.8 [46–48], whereas the isoelectric point of WO_3 is even lower and lies in the range 1.5–2.5 [49]. At higher pH values than these WO_3 and TiO_2 surfaces should be negatively charged. Therefore, the adsorption of the R6G as cationic dye at pH = 7, points out that the surfaces of WO_3/TiO_2 and TiO_2 coatings are negative and attract the positively charged R6G. The dye adsorption ability can be crucial for the high catalytic activity of the catalyst, because it can enhance the electron/hole transfer efficiency and contact with photogenerated active species.

When TiO_2 and WO_3/TiO_2 samples were subjected to visible radiation, composite coatings have shown much better photo-efficiency and demonstrated to be far superior than pure TiO_2. The highest activity was observed for the TW90 and TW120 samples for which the photodegradation of R6G reached almost 80% after 60 min. With further increase of WO_3 content, the photocatalytic efficiency slightly decreased, but is still much higher than for pure TiO_2.

Further, the photocatalytic activity of WO_3/TiO_2 coatings for degradation of MB9 was tested under the UV light. In Fig. 7b is presented the photodegradation of MB9 in the presence of WO_3/TiO_2 samples. In the dark, WO_3/TiO_2 coatings showed no adsorption of MB9. The absence of adsorption can be explained by highly anionic character of MB9 and electrostatic repulsion between the dye and negatively charged surface of WO_3/TiO_2 coatings.

The photocatalytic activity of WO_3/TiO_2 samples was improved with increased content of WO_3 phase, and the TW300 sample exhibited better activity than pure TiO_2. As can be seen from Fig. 7b, after 240 min more than 80% of dye was degraded in the presence of WO_3/TiO_2 coatings.

Photocatalytic degradation of both dyes can be well described by first-order kinetic equation, $ln(C/C_o) = kt$, where C_o is the initial dye concentration and C is the dye concentration at time t. The first order kinetic constant k is obtained from the slope of the $ln(C/C_o)$ versus t for both dyes. In Table 3 are given the first order rate constants for R6G and MB9 (k_{R6G}, k_{MB9}), together with the corresponding linear correlation coefficient (R^2). In a case of R6 G degradation under the visible light, the highest k value (k_{R6G}) was obtained for the TW90 sample. In a case of MB9 degradation under UV light, value of k_{MB9} increased with increasing amount of WO_3.

The degradation rate constant k of WO_3/TiO_2 coatings under visible light is almost five times higher than that of TiO_2, whereas its value under UV light are comparable with TiO_2, suggesting that

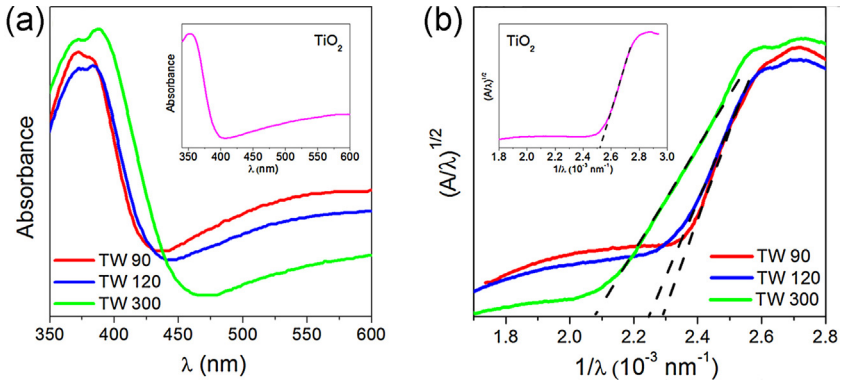

Fig. 5. Absorbance spectra (a) and Tauc plots for indirect band gap for WO_3/TiO_2 samples (b). In the inset is given Tauc plot for indirect band gap for pure TiO_2.

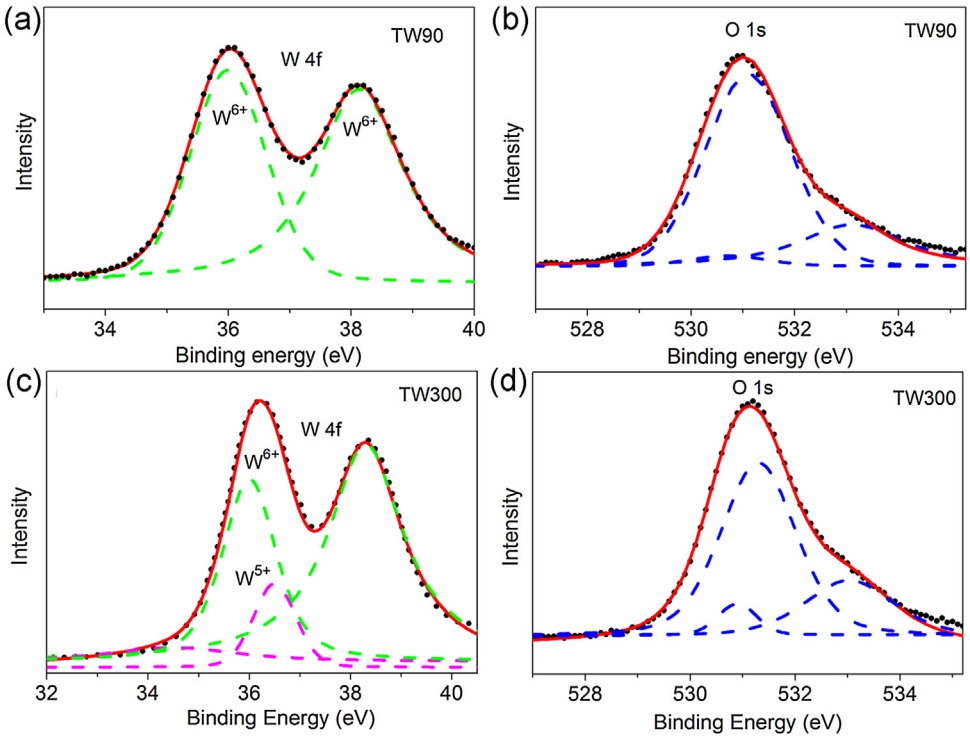

Fig. 6. XPS spectra of W 4f and O 1s regions for TW90 and TW300 samples.

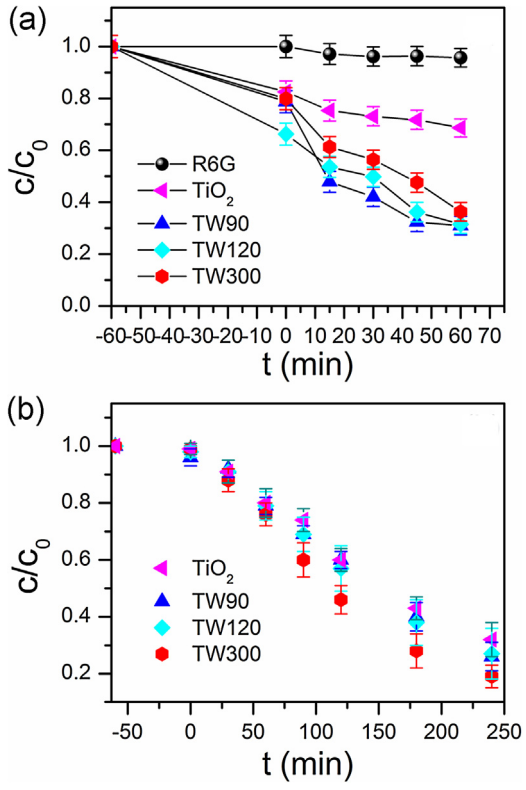

Fig. 7. Photocatalytic degradation of R6G under visible light (a) and MB9 under UV light (b) in the presence of WO_3/TiO_2 and TiO_2 coatings.

composite coatings are very efficient photocatalysts under visible light.

3.5. Hydroxyl radical analysis

The formation of free hydroxyl radicals ($OH^•$) was tested on the surface of TW300 photocatalyst under UV irradiation and detected by PL method. Applying similar procedure as described in the paper of Su et al. [50], TW300 sample was placed in terephthalic acid solution and illuminated by UV light. PL spectra of the reaction solution were measured at room temperature after 15, 30, 60 and 90 min, and these spectra are presented in Fig. 8. The terephthalic acid reacts with $OH^•$ producing 2-hydroxyterephthalic acid, which exhibits PL peak at 425 nm [51]. The intensity of this peak is proportional to the amount of $OH^•$ produced in water [50,51]. As can be seen from Fig. 8, gradual increase of PL intensity at 425 nm with prolonged illumination time points at increasing amount of $OH^•$ radicals produced at the surface of TW300 sample.

3.6. Mechanism of the reaction

The photocatalytic degradation of R6G or MB9 is initiated by the photoexcitation of the WO_3/TiO_2 coatings when the electron-hole pairs are formed on the catalyst's surface. According to the

Table 3
The pseudo-first rate constants for R6G and MB9 together with R^2.

Sample	$k_{R6G} \times 10^{-2}$ (min^{-1})	R^2	$k_{MB9} \times 10^{-2}$ (min^{-1})	R^2
TW90	1.52	0.975	0.44	0.990
TW120	1.24	0.957	0.47	0.982
TW300	1.20	0.963	0.65	0.966
TiO_2	0.28	0.888	0.41	0.963

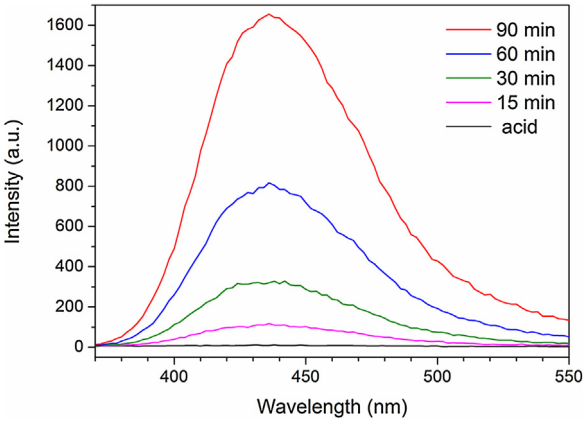

Fig. 8. PL spectral changes observed during UV illumination of TW300 sample in the solution of terephthalic acid after 15, 30, 60 and 90 min. The PL spectra of pure terephthalic acid is also presented.

generally accepted photoexcitation mechanism, electrons from the conduction band of TiO_2 can easily diffuse into the conduction band of WO_3 [40,52]. Since W(VI) can be easily reduced to W(V), WO_3 acts as an acceptor of conduction band electrons from TiO_2, whereas the photogenerated holes migrate in the opposite direction, i.e. from the lower-lying valence WO_3 band to the valence band of TiO_2. In such a way the charge separation efficiency can be increased.

In Fig. 9 is given an illustration of photo-induced electron-hole separation and reacting radicals formation. The presence of holes in the dye solution permits a direct oxidation of the dye, due to high oxidative potential of the holes (h^+):

$$h^+ + \text{dye} \rightarrow \text{dye}^{\bullet+} \rightarrow \text{oxidation of the dye} \quad (1)$$

Further, hydroxyl radicals ($OH^\bullet$) are usually formed by the reaction between the holes and OH^- or water molecules present on the surface of the catalyst. The $OH^\bullet$ radicals attack the dye in aqueous solution leading to its degradation:

$$OH^\bullet + \text{dye} \rightarrow \text{photodegradation of the dye} \quad (2)$$

The photo-induced electrons can also react with dissolved oxygen to form superoxide ions ($O_2^{-\bullet}$) which in contact with H_2O molecules form OH^- ions and finally $OH^\bullet$ radicals.

It is known from the literature that WO_3 is almost 15 times more acidic than TiO_2 [21,22,31], so it is expected that the surface of PEO produced WO_3/TiO_2 coatings is more acidic than that of TiO_2, and has a higher affinity for chemical species having unpaired electrons. Because of higher acidity, the surface of WO_3/TiO_2 coatings can absorb more H_2O and OH^- generating more $OH^\bullet$ radicals. The XPS and Raman spectra of WO_3/TiO_2 composite coatings gave an evidence that adsorbed H_2O and hydroxyls are present on the surface of WO_3/TiO_2 coatings, existence of which is important for the formation of $OH^\bullet$ radicals. PL measurements, performed on TW300 sample, (Fig. 8) clearly demonstrated that with increasing illumination time the increasing amount of $OH^\bullet$ radicals is formed on the surface of photocatalysts, which manifests through higher photocatalytic activity of TW300 sample.

The absorption measurements have shown that the band gap energy of TiO_2 is higher than that of WO_3/TiO_2 coatings. Namely, with prolonged time of PEO process, the WO_3 content increases followed by an appearance of $WO_{2.96}$ phase. As the conduction band of nonstoichiometric WO_{3-x} oxides is lower with respect to WO_3 and TiO_2 (Fig. 9) [53], the presence of $WO_{2.96}$ phase will further reduce the band gap of WO_3/TiO_2 samples towards the visible spectral range, as already noticed from the Tauc plots from Fig. 5. As a result, the electron-hole recombination will be more difficult and more reactive radicals can be produced at the WO_3/TiO_2 surface. Therefore, WO_3/TiO_2 coatings should be more efficient as catalysts under the visible light. The photocatalytic degradation of R6G and kinetics of the reaction confirmed that WO_3/TiO_2 coatings are efficient photocatalysts in the visible region. Slight decrease of photocatalytic activity of TW300 sample in a case of R6G photodegaradation (Fig. 7a) can be explained by the occurrence of photochromism [27,40]. Namely, the electron accumulation at the WO_3 conduction band can be more pronounced with increased WO_3 content. The accumulated electrons can react with $OH^\bullet$ radicals forming OH^- ions or can reduce the number of superoxide radicals [27,40] degrading at some extent the photocatalytic activity of WO_3/TiO_2 coatings. The presence of pronounced absorption feature around 380–400 nm in the absorbance spectrum of TW300 sample confirms this assumption. Another reason can be found in the formation of small polarons, appearance of which is characteristic for WO_3 and WO_{3-x} phases. The photoexcited electron-hole pairs can be rapidly quenched by recombination of photoexcited holes with electrons from localized polaron states, whereas photoexcited electrons

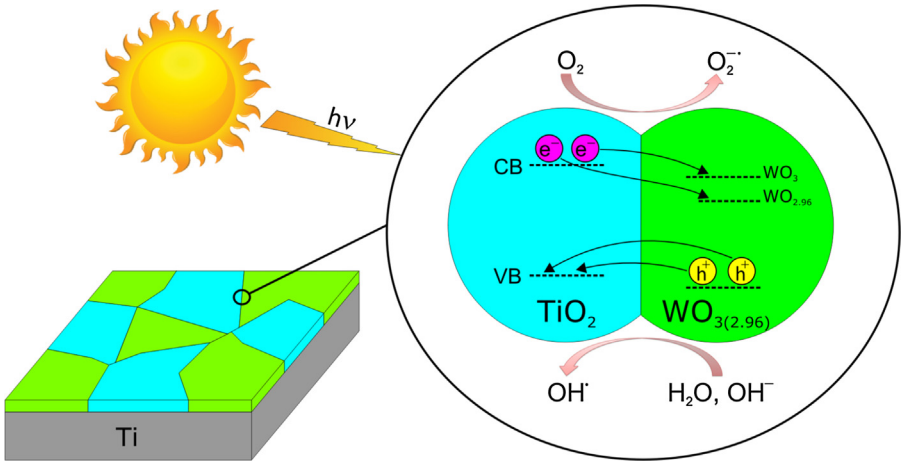

Fig. 9. Schematic diagram of electron-hole pairs separation and proposed mechanism of photodegradation over WO_3/TiO_2 photocatalysts.

populate polaron states [54], reducing on the other side the photocatalytic efficiency of the catalyst.

4. Conclusion

WO_3/TiO_2 composite and pure TiO_2 coatings have been prepared on titania substrates using facile and cost-effective PEO process. The structural, morphological, optical properties and chemical composition of these samples were investigated by different methods such as XRD, SEM, Raman, UV–vis diffuse reflectance spectroscopy and XPS. XRD and Raman analysis revealed that the coatings are mainly composed of monoclinic WO_3 and anatase TiO_2. With increasing duration of PEO process the crystallinity of the samples was improved, the WO_3 phase become dominant and a certain amount of monoclinic $WO_{2.96}$ phase appeared. XPS analysis confirmed the XRD results and revealed the presence of OH-groups and adsorbed H_2O on the surface of WO_3/TiO_2 coatings. The increasing amount of $WO_3/WO_{2.96}$ phase caused a decrease of optical band gap, i.e. shift from near UV to visible spectral region. The photocatalytic activity of WO_3/TiO_2 samples has been measured by monitoring photodecolouration of two model pollutants in aqueous solution, R6G under visible and MB9 under UV light irradiation. The WO_3/TiO_2 samples have shown enhanced photocatalytic activity compared to pure TiO_2 under the visible light irradiation. Slight decrease of photocatalytic activity under the visible light in the sample enriched with $WO_3/WO_{2.9}$ phase can be ascribed to the occurrence of photochromism and/or small polaron formation. Under the UV light, the WO_3/TiO_2 photocatalysts have shown slightly better photocatalytic activity than pure TiO_2. PL mesurements demonstrated the correlation between photoactivity and the formation rate of $OH^{\bullet}$ radicals under UV light irradiation, i.e. higher amount of $OH^{\bullet}$ radicals formed, the better photoactivity of WO_3/TiO_2 photocatalysts was achieved. The kinetics of the reaction in the case of both azo dyes followed the pseudo-first order. The degradation rate constant k of WO_3/TiO_2 coatings under the visible light is almost five times higher than that of TiO_2. Much better photocatalytic activity of the WO_3/TiO_2 samples compared to pure TiO_2 in the visible range can be attributed to better light absorption, higher adsorption affinity and increased charge separation efficiency with increasing content of $WO_3/WO_{2.96}$ phase.

Acknowledgements

This work was financially supported by the Ministry of Education, Science and Technological Development of the Republic of Serbia under the projects OI171032, III45018 and bilateral project Serbia-Italy No. RS13MO11.

References

[1] L. Ren, Y. Li, J. Hou, X. Zhao, C. Pan, ACS Appl. Mater. Interfaces 6 (2014) 1608–1615.
[2] F. Ruggieri, A.A. D'Archivio, M. Fanellia, S. Santucci, RSC Adv. 1 (2011) 611–618.
[3] M. Šćepanović, B. Abramović, A. Golubović, S. Kler, M. Grujić-Brojčin, Z. Dohčević-Mitrović, B. Babić, B. Matović, Z.V. Popović, J. Sol-Gel Sci. Technol. 61 (2012) 390–402.
[4] A. Golubović, B. Abramović, M. Šćepanović, M. Grujić-Brojčin, S. Armaković, I. Veljković, B. Babić, Z. Dohčević-Mitrović, Z.V. Popović, Mater. Res. Bull. 48 (2013) 1363–1371.
[5] S. Watson, D. Beydoun, J. Scott, R. Amal, J. Nanoparticle Res. 6 (2004) 193–207.
[6] A.N. Banerjee, Nanotechnol. Sci. Appl. 4 (2011) 35–65.
[7] M. Xing, D. Qi, J. Zhang, F. Chen, Chem. Eur. J. 17 (2011) 11432–11436.
[8] Y. Niu, M. Xing, J. Zhang, B. Tian, Catal. Today 201 (2013) 159–166.
[9] F. Ruggieri, D. Di Camillo, L. Maccarone, S. Santucci, L. Lozzi, J. Nanopart. Res. 15 (2013) 1–11.
[10] W. M. Xing, Y. Li, J. Wu, X. Gong Zhang, J. Phys. Chem. C 115 (2011) 7858–7865.
[11] M. Janus, B. Tryba, E. Kusiak, T. Tsumura, M. Toyoda, M. Inagaki, A.W. Morawski, Catal. Lett. 128 (2009) 36–39.
[12] M. Takeuchi, M. Matsuoka, M. Anpo, Res. Chem. Intermed. 38 (2012) 1261–1277.
[13] X. Chen, L. Liu, P.Y. Yu, S.S. Mao, Science 331 (2011) 746–750.
[14] W. Fang, M. Xing, J. Zhang, Appl. Catal. B: Environ. 160–161 (2014) 240–246.
[15] Y. Wang, J. Zhang, L. Liu, C. Zhu, X. Liu, Q. Su, Mater. Lett. 75 (2012) 95–98.
[16] Y. Xiaodan, W. Qingyin, J. Shicheng, G. Yihang, Mater. Charact. 57 (2006) 333–341.
[17] J. Rashid, M.A. Barakat, S.L. Pettit, J.N. Kuhn, Environ. Technol. 35 (2014) 2153–2159.
[18] B. Gao, Y. Ma, Y. Cao, W. Yang, J. Yao, J. Phys. Chem. B 110 (2006) 14391–14397.
[19] X. Luo, F. Liu, X. Li, H. Gao, G. Liu, Mat. Sci. Semicon. Proc. 16 (2013) 1613–1618.
[20] N.R. Khalid, E. Ahmed, Z. Hong, M. Ahmad, Y. Zhang, S. Khalid, Ceram. Int. 39 (2013) 7107–7113.
[21] Y. Li, P.C. Hsu, S.M. Chen, Sensor. Actuat. B-Chem. 174 (2012) 427–435.
[22] K.K. Akurati, A. Vital, J.P. Dellemann, K. Michalowa, T. Graule, D. Ferri, A. Baiker, Appl. Catal. B: Environ. 79 (2008) 53–62.
[23] D. Ke, H. Liu, T. Peng, X. Liu, K. Dai, Mater. Lett. 62 (2008) 447–450.
[24] H. Song, H. Jiang, X. Liu, G. Meng, J. Photoch. Photobio. A 181 (2006) 421–428.
[25] C. Shifu, C. Lei, G. Shen, C. Gengyu, Powder Technol. 160 (2005) 198–202.
[26] F. Riboni, L.G. Bettini, D.W. Bahnemann, E. Selli, Catal. Today 209 (2013) 28–34.
[27] J. Yang, X. Zhang, H. Liu, C. Wang, S. Liu, P. Sun, L. Wang, Y. Liu Catal, Today 201 (2013) 195–202.
[28] S. Bai, H. Liu, J. Sun, Y. Tian, S. Chen, J. Song, R. Luo, D. Li, A. Chen, C.-C. Liu, Appl. Surf. Sci. 338 (2015) 61–68.
[29] A. Rampaul, I.P. Parkin, S.A. O'Neill, J. DeSouza, A. Mills, N. Elliott, Polyhedron 22 (2003) 35–44.
[30] J.H. Pan, W. In Lee, Chem. Mater. 18 (2006) 847–853.
[31] M. Long, B. Tan, P. Hu, B. Zhou, Y. Zhou, J. Mater. Chem. A 3 (2015) 10195–10198.
[32] J. He, Q. Luo, Q.Z. Cai, X.W. Li, D.Q. Zhang, Mater. Chem. Phys. 129 (2011) 242–248.
[33] S. Stojadinović, N. Radić, R. Vasilić, M. Petković, P. Stefanov, Lj. Zeković, B. Grbić, Appl. Catal. B: Environ. 126 (2012) 334–341.
[34] S. Petrović, S. Stojadinović, Lj. Rožić, N. Radić, B. Grbić, R. Vasilić, Surf. Coat. Technol. 269 (2015) 250–257.
[35] T. Ohsaka, F. Izumi, Y. Fujiki, J. Raman Spectrosc. 7 (1978) 321–324.
[36] Y. Djaoued, S. Balaji, N. Beaudoin, J. Sol-Gel Sci. Technol. 65 (2013) 374–383.
[37] C. Santato, M. Odziemkowski, M. Ulmann, Jan Augustynski, J. Am. Chem. Soc. 123 (2001) 10639–10649.
[38] E. Cazzanelli, C. Vinegoni, G. Mariotto, A.J. Purans, Solid State Ionics 123 (1999) 67–74.
[39] Y. Yu, K. Lin, X. Zhou, H. Wang, S. Liu, X. Ma, J. Phys. Chem. C 111 (2007) 8971–8978.
[40] A.O.T. Patrocinio, L.F. Paula, R.M. Paniago, J. Freitag, D.W. Bahnemann, ACS Appl. Mater. Interfaces 6 (2014) 16859–16866.
[41] N. Ghobadi, Int. Nano Let. 3 (2013) 1–4.
[42] K. Senthil, K. Yong, Nanotechnology 18 (2007) 395604 (1–7).
[43] H. Ling, J. Lu, S. Phua, H. Liu, L. Liu, Y. Huang, D. Mandler, P.S. Lee, X. Lu, J. Mater. Chem. A 2 (2014) 2708–2717.
[44] A.P. Shpak, A.M. Korduban, V.O. Medvedskij, J. Electron. Spectrosc. Relat. Phenom. 156–158 (2007) 172–175.
[45] H.Y. Wong, C.W. Ong, R.W.M. Kwok, K.W. Wong, S.P. Wong, W.Y. Cheung, Thin Solid Films 376 (2000) 131–139.
[46] A.A. Khodja, A. Boulkamh, C. Richard, Appl. Catal. B: Environ. 59 (2005) 147–154.
[47] C.C. Wang, J.Y. Ying, Chem. Mater. 11 (1999) 3113–3120.
[48] M.D. Hernández-Alonso, F. Fresno, S. Suarez, J.M. Coronado, Energy Environ. Sci. 2 (2009) 1231–1257.
[49] M. Anik, T. Cansizoglu, J. Appl. Electrochem. 36 (2006) 603–608.
[50] T.M. Su, Z.L. Liu, Y. Liang, Z.Z. Qin, J. Liu, Y.Q. Huang, Catal. Comm. 18 (2012) 93–97.
[51] K. Ishibashi, A. Fujishima, T. Watanabe, K. Hashimoto, Electrochem. Commun. 2 (2000) 207–210.
[52] H. Park, A. Bak, T.H. Jeon, S. Kim, W. Choi, Appl. Catal. B: Environ. 115–116 (2012) 74–80.
[53] A.K.L. Sajjad, S. Shamaila, B. Tian, F. Chen, J. Zhang, Appl. Catal. B: Environ. 91 (2009) 397–405.
[54] M.B. Johansson, G.A. Niklasson, L. Österlund, J. Mater. Res. 27 (2012) 3130–3140.